Journal of Electronics, Electromedical Engineering, and Medical Informatics
Homepage: jeeemi.org; Vol. 8, No. 2, April 2026, pp: 638-656 e-ISSN: 2656-8632

RESEARCH ARTICLE OPEN ACCESS

Non-Contact Heart Rate Detection Using FMCW Radar Based on 1-D Convolutional Neural Networks

Diyah Widiyasari[1], Istiqomah[2], Fiky Yosef Suratman[3], and Suto Setiyadi [4]

[1] School of Electrical Engineering, Telkom University, Bandung 40257, Indonesia
[2] The University Center of Excellence Intelligent Sensing-IoT, Telkom University, Bandung 40257, Indonesia

Corresponding author: diyahwidiyasari@telkomuniversity.ac.id

Abstract **Non-contact heart rate (HR) estimation using frequency-modulated continuous-wave (FMCW) radar has emerged as a promising solution for unobtrusive, continuous vital-sign monitoring. However, accurately extracting HR from radar signals remains challenging because of low-amplitude cardiac-induced chest vibrations, environmental clutter, motion artifacts, and system noise. Traditional signal processing techniques, such as bandpass filtering combined with fast Fourier transform (FFT) analysis, are commonly employed to estimate HR in the frequency domain. Nevertheless, these approaches are highly sensitive to noise and often struggle to robustly capture weak cardiac components, leading to unstable or inaccurate estimates. To address these limitations, this study proposes a non-contact HR estimation framework based on FMCW radar combined with a one-dimensional convolutional neural network (1D-CNN). A systematic radar signal preprocessing pipeline is developed, including range-bin selection, phase extraction, noise suppression, filtering, and structured data labeling, to construct learning-ready input features. The 1D-CNN model is designed to automatically learn discriminative temporal patterns associated with cardiac activity directly from preprocessed radar signals. The proposed method is evaluated using two datasets: a publicly available dataset and an independently acquired dataset collected under controlled conditions. Performance is benchmarked against conventional bandpass filtering- and FFT-based HR estimation methods. The experimental results demonstrate that the proposed 1D-CNN framework achieves more accurate and stable HR predictions. On the public dataset, MAE decreases from 17.96 to 6.09 BPM, RMSE from 21.28 to 7.34 BPM, and MedAE from 17.66 to 5.43 BPM. The independent dataset yields consistent gains, with MAE decreases from 14.05 to 5.45 BPM, RMSE from 18.05 to 6.84 BPM, and MedAE from 10.74 to 4.57 BPM. These results indicate that the proposed 1D-CNN framework can effectively estimate HR from radar signals and demonstrate its capability to operate across datasets acquired with different radar frequencies.**

Keywords **FMCW radar; non-contact heart rate; 1D convolutional neural network; vital-sign monitoring; signal processing.**

I. Introduction

Vital-sign monitoring technologies have rapidly advanced in recent years. There are two main methods: contact-based and contactless systems. Monitoring vital signs is important for assessing overall health, cardiovascular function, and how the body responds to activity, stress, and disease [1]. Among various vital parameters, heart rate (HR) is one of the most fundamental and widely used indicators in both clinical and daily health monitoring. HR measurement is crucial for assessing human health. It is widely used in health monitoring, early detection of cardiovascular disorders, and evaluation of stress and fatigue, both in critical situations and daily life [2], [3], [4], [5]. Most current heart rate measurements rely on contact-based methods, such as electrocardiography (ECG) and photoplethysmography (PPG), which record the heart's electrical activity or blood-volume pulse signals using wearable sensors. Although these approaches provide high accuracy, they suffer from several limitations, including potential allergic reactions due to prolonged skin contact, discomfort during electrode removal, and restricted user mobility during long-term monitoring [6], [7], [8], [9].To address the drawbacks of contact-based HR measurement methods, numerous studies have explored contactless HR detection technologies. Among these, camera-based approaches have been extensively investigated; however, they are highly sensitive to environmental conditions and raise privacy concerns [10], [11],

Manuscript received 13 February 2026; Revised 6 April 2026; Accepted 8 April 2026; Available online 11 April 2026
Digital Object Identifier (**DOI**): https://doi.org/10.35882/jeeemi.v8i2.1547

[12], [13]. To overcome these issues, radar technology has emerged as a promising alternative [6]. Among contactless sensing methods, millimeter-wave (mmWave) radar is a promising technology for monitoring vital signs. mmWave radiation is non-ionizing, is absorbed by superficial skin tissues, and causes only thermal effects. According to international safety standards (e.g., IEEE C95.1) for radio-frequency electromagnetic fields (0 Hz–300 GHz), reported mmWave exposure levels for sensing remain within recommended limits. Under typical operating conditions, mmWave radar-based physiological monitoring is safe for humans [14], [15], [16]. Radar technologies are classified by signal type as continuous-wave (CW), frequency-modulated continuous-wave (FMCW), and ultra-wideband (UWB) [17]. This technology offers robustness to lighting variations and improved privacy protection [18], [19], [20]. Specifically, frequency-modulated continuous-wave (FMCW) radar has gained significant attention for offering high accuracy and relatively low power consumption compared to other radar systems [10], [11], [21]. Despite these advantages, radar-based heart rate detection still faces several challenges.

One main difficulty is detecting the extremely weak chest micromotions associated with heartbeats. These signals are often masked by respiration and other body movements [21], [22], [23], [24], [25]. This overlap makes accurate signal separation particularly challenging. To address this issue, several studies have proposed advanced signal-processing techniques. Wang et al. employed a 77-GHz FMCW radar to analyze the phase of the intermediate-frequency (IF) signal. They used compressive sensing orthogonal matching pursuit (CS-OMP) and range-adaptive discrete wavelet transform (RA-DWT), followed by frequency estimation and autocorrelation, to extract HR and respiration rate (RR) signals [22]. Similarly, Chen et al. proposed a method combining median filtering and the DR-MUSIC algorithm, which integrates recursive least squares (RLS) with multiple signal classification (MUSIC), to separate heartbeat and respiration signals using a 77-GHz FMCW radar [11]. Another approach by Lv et al. used a 120-GHz FMCW radar with a narrow-beam antenna to improve signal-to-noise ratio (SNR). They also applied adaptive notch filtering and a modified fast Fourier transform (FFT) to enhance detection accuracy [26]. Xue et al. combined moving target indication (MTI), constant false alarm rate (CFAR) detection, and K-means clustering with an extended differentiate-and-cross-multiply phase demodulation algorithm to suppress clutter and enable accurate multi-target vital-sign detection using a 77-GHz FMCW radar [23]. Yuan et al. proposed a Gaussian mean filtering decomposition (GMFD)-based method to enhance the accuracy and stability of contactless vital sign detection using FMCW radar [27].

Besides conventional and adaptive filtering techniques, machine-learning-based methods have recently been explored for HR and RR detection. For example, Saluja et al. applied a supervised learning-based gamma filter to a 5.8-GHz Doppler radar. This approach enabled real-time heartbeat detection without additional calibration, using modified ECG signals as training data [28]. Similarly, El Abbaoui et al. developed a contactless physiological monitoring approach using a 24-GHz continuous-wave (CW) radar and various temporal neural network (T-CNN) architectures. These included one-dimensional convolutional neural networks (1D-CNN), temporal convolutional networks (TCN), bidirectional long short-term memory (Bi-LSTM), and convolutional recurrent neural networks (CRNN) to classify drivers' physiological conditions. Although the CRNN approach showed superior performance, evaluation was limited to simulated data, indicating a need for further validation in real-world dynamic environments [7]. Previous studies have reported deep learning approaches for radar-based heart rate estimation using millimeter-wave signals. These approaches use CNN to address weak heartbeat signals affected by respiratory harmonics and environmental noise. By decomposing phase signals via empirical wavelet transform (EWT) and employing lightweight, depthwise convolution architectures, higher estimation accuracy is achieved than with conventional methods [29]. 1D-CNN is widely used in bioinformatics for DNA sequence classification and protein structure prediction, as well as in finance, healthcare, and manufacturing [30]. Most 1D-CNN applications address classification tasks. For example, Khan et al. classified ECG signals using raw heartbeats [31]. Similarly, Narotamo et al. investigated deep learning-based ECG classification for cardiovascular disease diagnosis by comparing multiple ECG representations and network architectures, including 1D-CNN, RNN-based models, and 2D-CNN [32]. However, beyond classification, 1D-CNN are inherently well suited for regression-based physiological parameter estimation because they learn hierarchical temporal features that capture subtle amplitude and phase variations embedded in time-series signals [33]. Based on these considerations, this study proposes a HR estimation method based on 1D-CNN operating on FMCW radar signals. The 1D-CNN architecture is chosen for its suitability in processing sequential data, effectively

Manuscript received 13 February 2026; Revised 6 April 2026; Accepted 8 April 2026; Available online 11 April 2026
Digital Object Identifier (**DOI**): https://doi.org/10.35882/jeeemi.v8i2.1547

extracting local temporal patterns and inter-sample dependencies. This study proposes a regression-based 1D-CNN framework for continuous heart rate estimation from FMCW radar phase signals. The proposed architecture operates on temporal radar phase data and directly estimates HR values in beats per minute (BPM), rather than performing categorical classification. A publicly available 60-GHz FMCW radar dataset collected in a vehicular environment is utilized [34] and the approach is further validated using an independent 77-GHz FMCW radar platform (Texas Instruments IWR1843BOOST). The contributions of this paper are as follows:

1. A regression-based 1D-CNN model for continuous HR estimation directly from FMCW radar phase signals.
2. The proposed 1D-CNN automatically extracts features from temporal radar signals and maps them directly to BPM, eliminating manual intervention.
3. The proposed 1D-CNN is validated on two independent datasets: a public 60 GHz FMCW radar dataset and a self-acquired 77 GHz FMCW radar dataset.

The rest of this paper is organized as follows. Section II describes the proposed 1D-CNN-based HR estimation method, including preprocessing and dataset segmentation. Section III presents the experimental results and evaluation. Section IV discusses the findings, compares them with existing methods, and notes limitations. Section V provides the conclusion.

II. Method

A. System Overview

In this study, 1D-CNN is used as a regression model. It estimates HR in BPM from FMCW radar signals after preprocessing. The 1D-CNN is not used for classification. Instead, it directly maps time-domain radar signals to a single BPM value. The public dataset used in this study has two types of data [34]. It contains FMCW radar signals and reference HR data from ECG sensors. The ECG reference data are preprocessed into BPM values, which serve as ground truth during model training and evaluation. Fig. 1 presents the overall processing pipeline of the proposed system. Of the 50 subjects in the public dataset [34], 47 are used for training and testing. The remaining three subjects are reserved as unseen test data. Data from these three subjects are excluded from the training set. They are used to assess the model's generalization for estimating HR in previously unobserved individuals.

The FMCW radar signals from each subject are first processed through several stages to extract heartbeat-related components. These stages include fast Fourier transform (FFT), moving target indication (MTI), phase extraction, bandpass filtering, and signal normalization. The preprocessing steps enhance HR-related signal quality while suppressing noise and other disturbances. After preprocessing, the radar signals are segmented using a sliding-window approach. Each window lasts 20 seconds and has a sampling frequency of 20 Hz, yielding 400 signal samples per segment. Each segment is paired with a single BPM value from the ECG reference data over the same time interval. As a result, each radar segment of 400 samples is associated with one HR label in BPM. This labeling scheme is used for the training, testing, and prediction datasets. This approach enables the 1D-CNN to learn the relationship between temporal patterns in radar signals and HR values. It uses a one-to-one

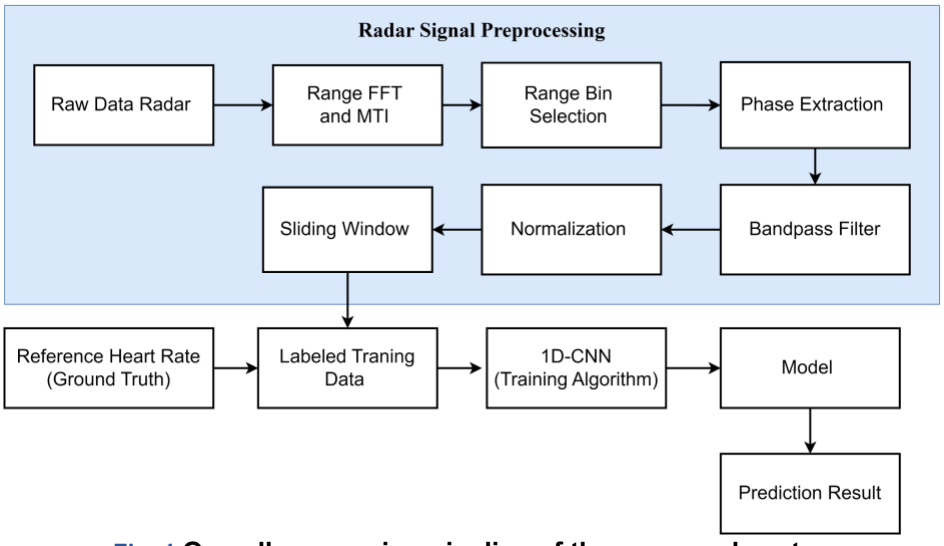

Fig. 1 Overall processing pipeline of the proposed system

Manuscript received 13 February 2026; Revised 6 April 2026; Accepted 8 April 2026; Available online 11 April 2026
Digital Object Identifier (**DOI**): https://doi.org/10.35882/jeeemi.v8i2.1547

regression framework, in which each radar segment serves as input and each BPM value serves as output. During training, several 1D-CNN models are evaluated. The model with the highest coefficient of determination (R^2) is selected. This model is then used to predict HR values on test data from two sources: three subjects from the public dataset and three adult subjects whose data were collected independently using an FMCW radar module (IWR1843BOOST, 77 GHz).

B. FMCW Radar Working Principle

FMCW radar transmits a continuous electromagnetic wave signal whose frequency changes linearly over time to measure distance, angle, and velocity. This type of radar consists of key components such as transmit (Tx) and receive (Rx) antennas, power amplifier (PA), low-noise amplifier (LNA), analog-to-digital converter (ADC), digital signal processor (DSP), and filters [22], as shown in the block diagram in Fig. 2. In its application for detecting vital signs such as HR, the radar captures signals reflected from chest wall movements during breathing and cardiac activity. In FMCW radar, the frequency-modulated signal is called a chirp.

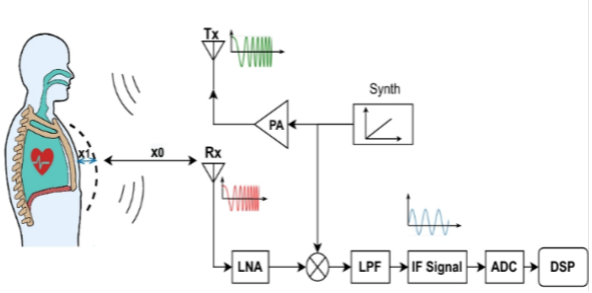

Fig. 2 Block diagram FMCW radar

The equation for the transmitted signal is expressed in Eq. (1) [22], [34], [35]. The FMCW radar transmits a periodic signal $x_T(t)$ with a frequency that increases linearly over time. Here, f_c denotes the starting frequency of the transmitted signal, A_T represents the amplitude of the transmitted signal, T_c is the chirp duration, and B is the signal bandwidth. The chirp slope μ is defined as $\mu = B/T_c$. After transmission, the signal is reflected by the target, resulting in a received signal denoted as $x_R(t)$. This received signal is expressed in Eq. (2).

$$x_T = A_T \cos(2\pi f_c t + \pi\mu t^2) \quad (1)$$

$$x_R = A_R \cos(2\pi f_c(t - t_d) + \pi\mu(t - t_d)^2) \quad (2)$$

where A_R denotes the amplitude of the received signal and t_d represents the time delay. Eq. (2) describes the delayed and attenuated version of the Tx signal given in Eq. (1). In the next stage, the Tx and Rx signals are mixed to generate an intermediate-frequency (IF) signal. The resulting IF signal, denoted as $x_{IF}(t)$, is expressed in Eq. (3). and Eq. (4).

$$x_{IF} = x_T(t) \times x_R(t) \quad (3)$$

$$x_{IF} = A_{IF} \exp[j(2\pi f_c t_d + 2\pi\mu t_d t - \pi\mu {t_d}^2)] \quad (4)$$

where A_{IF} is the amplitude of the IF signal, and $t_d = {2d}/{c}$, c represent the light speed. The quadratic term $\pi\mu {t_d}^2$ has a very small contribution and can therefore be neglected [29]. Consequently, the IF signal can be expressed in a simplified form, as shown in Eq. (5), where f_{IF} denotes the intermediate beat frequency that encodes the target distance.

$$x_{IF} = A_{IF} \exp[j(2\pi f_{IF} t + \varphi)] \quad (5)$$

$$f_{IF} = \mu t_d = \frac{2Bd}{cT_c} \quad (6)$$

$$\varphi = 2\pi f_c t_d = \frac{4\pi f_c d}{c} = \frac{4\pi d}{\lambda} \quad (7)$$

where λ denotes the radar wavelength. This relationship indicates that the IF frequency contains information about the target distance [34] while the phase of the IF signal (φ) is highly sensitive to small variations in distance [22], [29], [35]. As a result, it can be exploited to detect minute chest displacements caused by cardiac activity. These relationships are shown in Eq. (6). and Eq. (7).

C. Dataset Description

In this study, two types of data are employed, namely a public dataset and self-acquired data. The public dataset is used as training data to build a model that predicts HR in BPM from radar signals [34]. Subsequently, the self-acquired radar data are used as an independent test dataset to evaluate the model's generalization capability, particularly across different radar configurations and operating frequencies, while applying the same preprocessing procedures. This evaluation aims to determine whether the proposed model can still provide accurate HR estimates when applied to radar data with different characteristics.

1. Public FMCW Radar Dataset

This study employs a public FMCW radar dataset for the detection of HR and RR in children aged under 13 years, comprising 50 subjects [34]. The data acquisition system utilizes an FMCW radar sensor (IWR-6843), operating at 60 GHz as the primary sensing device, and a clinical reference sensor (BSM6501K) as the ground-truth measurement of vital signs. The dataset provides raw radar signal data, reference HR values (BPM), and recorded ECG signals.

Each subject is recorded for 5 minutes (300 seconds). The radar system operates at a frame rate

Manuscript received 13 February 2026; Revised 6 April 2026; Accepted 8 April 2026; Available online 11 April 2026
Digital Object Identifier (**DOI**): https://doi.org/10.35882/jeeemi.v8i2.1547

of 20 Hz, meaning that 20 frames are captured per second. Therefore, for a 5-minute recording duration, each subject contains a total of 6000 frames. Each frame consists of two chirps, and each chirp contains 512 samples. The detailed radar configuration parameters are summarized in Table 1. Timestamp information is obtained from both the radar measurements and the clinical reference sensor to ensure proper temporal alignment.

Table 1. Radar Dataset Configuration

Parameter	Value
Number of Tx	1
Number of Rx	4
Starting Frequency (f_c)	60.25 GHz
Bandwidth	3.75 GHz
Number of chirps per-frame	2
Frame rate	20 Hz
Samples per-chirp	512

Synchronization between radar signals and reference measurements is conducted using the HR values in BPM provided within the dataset. Although raw ECG signals were available, HR is not recalculated from the ECG waveform. Instead, the provided HR values are employed as ground truth. These HR values are temporally aligned with the corresponding radar signals using the available timestamp data.

2. Self-Acquired FMCW Radar Dataset

In addition to the public dataset, self-acquired data are collected using an FMCW radar system of type IWR-1843BOOST. The IWR-1843BOOST is an integrated mmWave sensor based on FMCW radar technology, capable of operating in the 76–81 GHz frequency range with a bandwidth of up to 4 GHz. To enable raw data acquisition from the FMCW radar, an additional module, namely the DCA1000EVM, is employed. The radar configuration utilizes one Tx and four Rx antennas. This configuration is selected because the target of interest is a single subject, while the use of four receive antennas is intended to improve measurement accuracy. In FMCW radar systems, a transmitted signal with linearly varying frequency is referred to as a chirp, whereas a set of chirps used as an observation window for radar signal processing is referred to as a frame. The detailed radar configuration parameters are summarized in Table 2.

During data acquisition, each frame consists of two chirps, and each chirp contains 200 samples. The data are recorded for 2 minutes (120 s), resulting in a total of 2400 frames, using combined signals from the four receive antennas. The subject is positioned 0.5 m in front of the radar sensor during data acquisition. Data are collected from three healthy subjects, comprising one male and two females aged 22-29 years. One subject is classified as overweight and obese class I based on body mass index (BMI), while the remaining subjects are within the normal BMI range. A Polar H10 sensor is used as the reference device for HR measurement.

Table 2. FMCW Radar Configuration for Vital Sign Extraction

Parameter	Value
Number of Tx	1
Number of Rx	4
Starting Frequency (f_c)	77 GHz
Number of chirps per-frame	2
Frequency Slope	70 MHz/ μs
Bandwidth	4 GHz
Frame rate	20 Hz
Samples per-chirp	200
Frame time	50 ms
Number of frames	2400
Chirp time	50 μs

D. Radar Signal Preprocessing

1. Extract Range Profile

After the received signal is processed by the ADC and other preliminary processing stages, the raw data are represented as a two-dimensional matrix consisting of fast-time and slow-time dimensions. The fast-time and slow-time dimensions correspond to different temporal scales in FMCW radar data acquisition and analysis. An illustration of this data structure is shown in Fig. 3. The vertical axis of the matrix corresponds to the fast-time samples, determined by the number of samples per chirp (N), while the horizontal axis corresponds to the slow-time samples, determined by the number of frames (M). Before extracting the subject profile, a direct current (DC) removal process is applied. DC removal aims to eliminate or suppress the DC component from the received radar signal. The radar signal is reflected not only by the subject but also by surrounding objects within the radar coverage area, such as walls and floors. These objects typically have a larger radar cross section than the human target, thus contributing significantly to the received signal power. The DC removal process is performed by subtracting the mean value of the fast-time samples in each frame from the corresponding data samples.

To obtain the range information of the target, an FFT process is employed. This process is referred to as range FFT because it utilizes the FFT to estimate the target distance from the radar. The FFT converts the sampled complex or intermediate-frequency (IF) signal from the time domain into the frequency domain. The FFT is applied to the fast-time samples of each chirp. During radar data acquisition, reflections from stationary objects in the surrounding

Manuscript received 13 February 2026; Revised 6 April 2026; Accepted 8 April 2026; Available online 11 April 2026
Digital Object Identifier (**DOI**): https://doi.org/10.35882/jeeemi.v8i2.1547

environment generate static clutter. This interference distorts the signal and degrades the detection of moving targets, particularly chest motion induced by respiration and heartbeat.

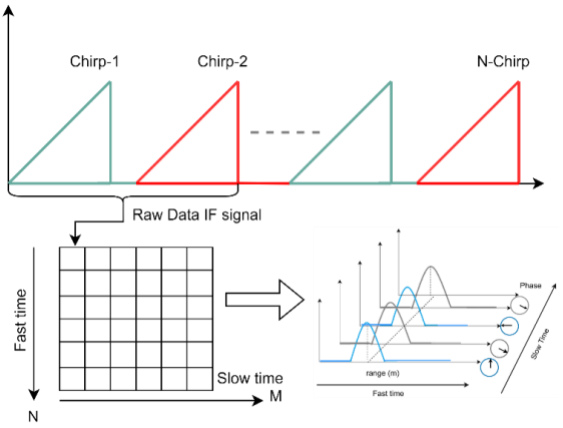

Fig. 3 Representation of FMCW radar data structure

To mitigate this effect, a moving target indication (MTI) process is employed to distinguish moving targets from stationary targets and clutter [36], [37]. In general, two MTI approaches are widely used: FIR- and IIR-based filters [38]. In this study, a first-order infinite-impulse-response (IIR) filter is adopted. The use of an IIR filter is motivated by the small Doppler frequency difference between stationary and moving targets. This process facilitates the extraction of respiration and HR information. Since heartbeat signals are weak and highly susceptible to noise, the MTI stage is essential. The MTI process is applied to each range FFT output, and the corresponding MTI equations are given in Eq. (8) and Eq. (9).

$$X_c[M,N] = (\alpha R_{fft}[M,N] + ((1-\alpha)\, X_c[M,N-1]) \quad (8)$$

$$R_{fft}[M,N] = R_{fft}[M,N] - X_c[M,N] \quad (9)$$

Where X_c denotes the clutter signal over the slow-time dimension (M) during data acquisition, and α represents the filter gain coefficient, which typically satisfies $0 < \alpha < 1$, in this study $\alpha = 0.01$ is used. Subsequently, R_{fft} represents the range FFT output computed from the fast-time samples for all data frames [34], [38]. After obtaining the cleaned signal, a range-bin selection criterion is applied to identify the bin corresponding to the maximum magnitude within the expected target distance range. In this study, a target distance of 0.5 m is used consistently for both the public dataset and the self-acquired data.

2. Phase Extraction

Phase extraction is a process for obtaining phase information from radar signals. This phase information is utilized to detect the heartbeat signal. The phase extraction process is performed after the subject location has been identified. Although several methods can be employed to extract phase information, previous studies have demonstrated that the differential-and-cross-multiply (DACM) algorithm provides superior performance in handling phase ambiguity [21], [22], [39]. Phase jumps typically occur when the arctangent demodulation method is employed, since this method has a limited output range, usually $(-\pi/2, \pi/2)$ or $(-180^{\circ}, 180^{\circ})$. W When the phase value exceeds this range, a phase jump occurs, leading to the loss of true phase information. The phase extraction equation is given in Eq. (10) [21].

$$\varphi(m) = \sum_{k=2}^{m} \frac{I(k)\big(Q(k)-Q(k-1)\big) - Q(k)\big(I(k)-I(k-1)\big)}{I^2(k)+Q^2(k)} \quad (10)$$

where $\varphi(m)$ denotes the phase information, $I(k)$ and $Q(k)$ represent the real and imaginary components of the signal obtained after the MTI process, and m denotes the number of samples. After phase extraction, impulse noise often appears due to interference and wave superposition, particularly when the phase approaches $-\pi$ and π. To suppress this impulse noise, a noise removal process is applied. This process computes the forward and backward phase differences for each data sample to reduce impulsive noise.

3. Bandpass Filter and Normalization

A bandpass filter is applied to the FMCW radar signal to isolate heartbeat components. Two HR cutoff frequency ranges are defined by age: for children under 13 years in the public dataset, HR is 60–150 bpm, and for adults aged 20 years and above, HR is 60–100 bpm [40]. HR values are converted to frequency in Hz using $f(Hz) = HR/60$, since bpm denotes beats per minute. Accordingly, the filtering frequency band for the public dataset is set to 0.8–3 Hz [22], [38]. The bandpass filter is implemented as a sixth-order Butterworth filter using the SciPy function in Python. To ensure numerical stability, the filter is implemented in second-order-section (SOS) form. Zero-phase filtering is performed using the sosfiltfilt function, which applies forward and backward filtering to eliminate phase distortion. This approach preserves the temporal structure of the phase signal while effectively suppressing low-frequency drift and high-frequency noise. After filtering, a normalization step is applied before performing sliding-window segmentation or dividing the signal into multiple segments. Normalization is employed to scale the

Manuscript received 13 February 2026; Revised 6 April 2026; Accepted 8 April 2026; Available online 11 April 2026
Digital Object Identifier (**DOI**): https://doi.org/10.35882/jeeemi.v8i2.1547

signal to a uniform range. In this study, the selected normalization method maps the signal to the range of 0 to 1. The normalization equation is given in Eq. (11).

$$\hat{x}_i = \frac{x_i - x_{min}}{x_{max} - x_{min}}, x_{max} \neq x_{min} \quad (11)$$

where x_i denotes the value of the i-th data sample before normalization, while $\hat{x}_i$ represents the value of the i-th data samples after normalization. The terms x_{min} and x_{max} indicate the minimum and maximum values of the entire data. In the case where x_{min} = x_{max}, all data values are set to zero.

4. Sliding Window

After the normalization process, sliding-window segmentation is applied. Previous studies have reported window durations of 5–60 seconds [22], [41], [42]. In this study, a 20-second window is selected to balance biological stability and temporal responsiveness. The observed HR range is approximately 60–150 BPM. A 20-second segment contains approximately 20–50 cardiac cycles. This provides sufficient periodic information for stable HR representation. Shorter windows, such as 5–10 seconds, may contain too few cardiac cycles. This increases sensitivity to noise and transient fluctuations. Longer windows improve stability but reduce responsiveness to HR changes.

With a sampling frequency of 20 Hz, each 20-second window consists of 400 consecutive samples. Each window produces one HR estimate. A one-second shift does not mean that HR is computed from only one second of data. Instead, it enables the model to update HR predictions every second using overlapping 20-second windows. This method maintains estimation stability while providing continuous temporal updates. There are 6000 samples per subject in the public dataset. This configuration produces 280 windowed segments per subject. These segments are then paired with the corresponding HR labels for supervised regression modeling. Fig. 5 shows the sliding-window process at 20-second intervals.

5. Labeled Training Data

After preprocessing, the radar signal for each subject is segmented using a 20-second sliding window advanced by a 1-second step. At a sampling frequency of 20 Hz, each window contains exactly 400 samples, yielding approximately 280 windows per subject. Once segmentation is complete, each windowed segment is aligned with its corresponding heart rate value through a timestamping procedure. Since the dataset measurement protocol includes an initial 20-second stabilization period, reference HR values are extracted starting from the 21st second onward, ensuring that every window is paired with a

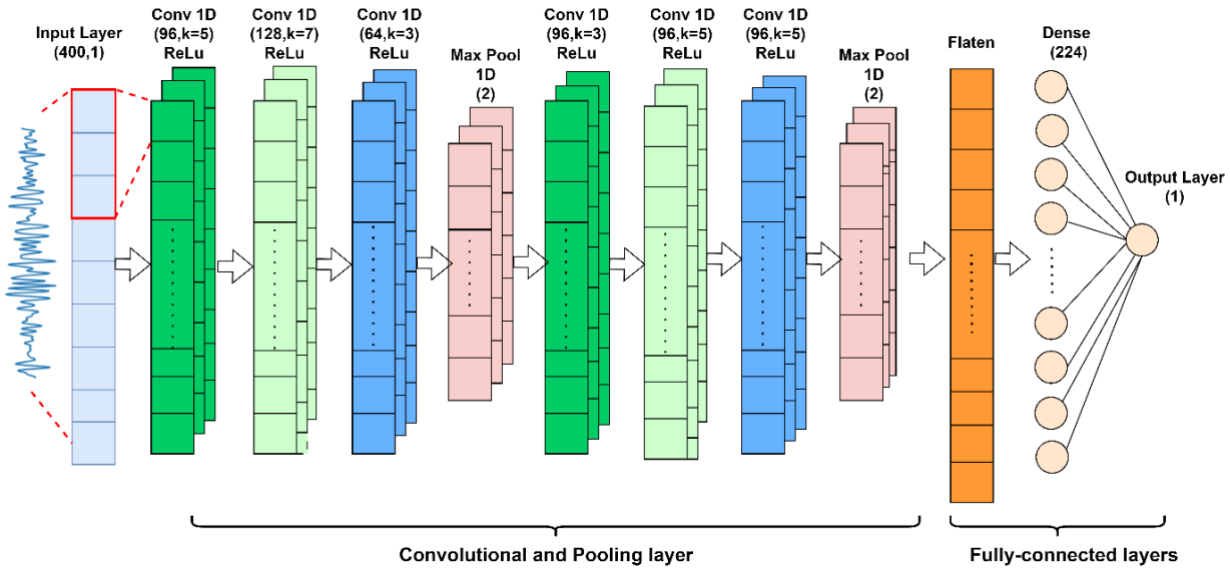

Fig. 4 The proposed 1D-CNN model.

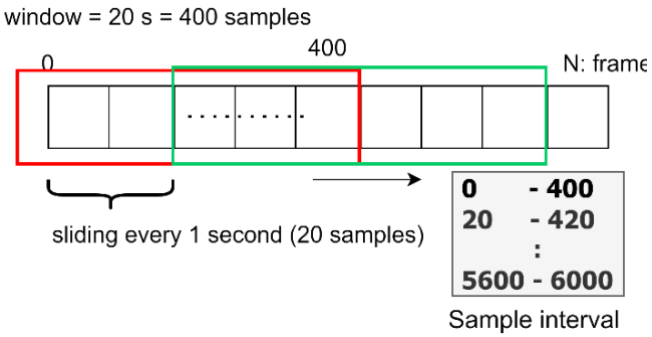

Fig. 5 Sliding window process.

Manuscript received 13 February 2026; Revised 6 April 2026; Accepted 8 April 2026; Available online 11 April 2026
Digital Object Identifier (**DOI**): https://doi.org/10.35882/jeeemi.v8i2.1547

temporally valid BPM label rather than one drawn from the unstable early phase. Each segment is then assigned a single BPM value as its label, producing instance pairs of 400 radar samples and one HR reference value. Across all 47 development subjects, this process yields approximately 13,160 labeled instances. The labeled windows from all subjects are then aggregated into a single dataset. The dataset is subsequently partitioned at the window level using the scikit-learn's train_test_split function with an 80%–20% split and random state, allocating 38 subjects (roughly 10,640 windows) to the training set and 9 subjects (roughly 2,520 windows) to the validation set. The remaining 3 subjects are held out entirely as an unseen test set to evaluate the model's generalization capability.

E. 1D-CNN Architecture

The proposed 1D-CNN is designed to map one-dimensional input signals to heart rate values expressed in BPM. The input signal has a length of 400 samples with a single channel (400 × 1). The network consists of multiple one-dimensional convolutional layers, two pooling layers, and a fully connected layer that produces a single output value. This hierarchical architecture enables the model to extract temporal features from the input signal at multiple levels of abstraction, yielding feature representations relevant to heart rate estimation. Since the model output is a single continuous value, the proposed method formulates the heart rate estimation task as a regression problem.

1. Convolutional Layer

1D-CNNs process one-dimensional data, such as time-series signals. They are also used for single-axis data, including audio, physiological, and sensor data. In contrast, two-dimensional CNNs (2D-CNNs) process data with two spatial axes, such as digital images. Three-dimensional CNNs (3D-CNNs) handle data spanning three axes, for example, image sequences or video [30]. In a 1D-CNN, the convolution operation consists of sliding a small filter, or kernel, along a single axis of the input data. The input is typically a sequence or time series. The kernel, comprising a set of weights, is designed to detect specific local signal characteristics, such as oscillations and periodic patterns. This operation enables the network to capture temporal information regarding changes in the data over time. It transforms these patterns into representative features that are learned during training [30], [43]. The general form of the convolution operation in a convolutional neural network is presented in Eq. (12).

$$(x * h)(t) = \sum_{j=0}^{k-1} x(t+j).h(j) \quad (12)$$

Where x denotes the input data and h represents the convolution kernel of size k. The kernel is moved along a single axis of the input vector to perform the convolution operation, as indicated by $(x * h)(t)$ [30], [41], [43]. In this study, the convolution operation is implemented across the Conv1D layers. Six Conv1D layers are employed in a hierarchical arrangement. Each convolutional layer uses the Rectified Linear Unit (ReLU) activation function, and the kernel size is selected from the set {3, 5, 7} through hyperparameter tuning using Keras Tuner. The number of filters in each layer is optimized within the range of 32 to 128, with increments of 32. As shown in Fig. 4. the initial convolutional layers (Conv1–Conv3) slide kernels along the temporal axis of the signal to extract fundamental patterns, including small oscillations and amplitude fluctuations relevant to heart rate signals. The subsequent convolutional layers (Conv4–Conv6) integrate these features to generate higher-level and more informative representations.

2. Pooling Layer

The pooling layer reduces the dimensionality of the feature maps produced by the convolutional layers while preserving the most relevant information. Like the convolution operation, pooling applies a sliding window to a specific region of the input feature map with a given stride and then transforms the values within that region into a single representative value. Two common pooling methods are max pooling and average pooling [19], [20], [21]. In this study, max pooling with a pool size of 2 is used. The pooling operation is mathematically expressed in Eq. (13).

$$\mathrm{y(t)} = max(x_i)_{i=0}^{N} \quad (13)$$

Where $y(t)$ is the output of the pooling layer, and x_i extends to the input feature map signal, and N is the number of elements in the pooling.

3. Fully Connected Layer

After passing through the sequence of convolutional and pooling layers, the resulting feature maps are transformed into a one-dimensional vector using a flatten layer [30]. This vector is then processed by a dense (fully connected) layer, with the number of neurons optimized through hyperparameter tuning within the range of 32 to 256. The fully connected layer integrates all extracted temporal features into a single global representation of the input signal. This representation is subsequently used to map the extracted features to the heart rate output value. At the final stage, a single neuron in the output layer is used without a nonlinear activation function to produce a single continuous output value, namely, the estimated heart rate in BPM.

4. Activation Function

Manuscript received 13 February 2026; Revised 6 April 2026; Accepted 8 April 2026; Available online 11 April 2026
Digital Object Identifier (**DOI**): https://doi.org/10.35882/jeeemi.v8i2.1547

The activation function used in all convolutional layers and the dense layer is the Rectified Linear Unit (ReLU). This function introduces nonlinearity into the network, enabling the model to learn complex relationships between the input signal and heart rate. In the output layer, no nonlinear activation function is applied because the model is designed to produce a single continuous value, consistent with the regression task formulation. The general form of the ReLU activation function is given in Eq. (14) [30].

$$f(z) = \begin{cases} z, & z > 0 \\ 0, & z \leq 0 \end{cases} \quad (14)$$

where z denotes the linear output of a neuron before activation. The ReLU function sets negative input values to zero while preserving positive values and its output is the maximum of zero and the input value z.

F. Evaluation Metrics

The performance of the proposed method is evaluated using a comprehensive set of metrics. As the developed 1D-CNN model is formulated as a regression task, Mean Squared Error (MSE) is employed as the loss function during training due to its differentiability, which facilitates gradient-based optimization. Furthermore, MSE imposes a greater penalty on larger errors, encouraging the model to minimize significant deviations.

For post-hoc evaluation, Root Mean Squared Error (RMSE) is reported to express the prediction error in the same unit as heart rate (BPM), allowing for direct clinical interpretation while maintaining sensitivity to large deviations. Mean Absolute Error (MAE) is also utilized to measure the average absolute difference, providing a straightforward baseline of estimation error. To further mitigate the influence of extreme outliers, Median Absolute Error (MedAE) is included to represent the typical error magnitude in a robust manner.

Finally, the Coefficient of Determination (R^2) is adopted to quantify the model's ability to explain the variance in the reference data. A higher R^2 value, approaching unity, indicates superior predictive performance. The mathematical definitions of these evaluation metrics are provided in Eq. (15-19).

$$MSE = \frac{1}{N}\sum_{i=1}^{N}(y_i - \hat{y}_i)^2 \quad (15)$$

$$MAE = \frac{1}{N}\sum_{i=1}^{N}|y_i - \hat{y}_i|^2 \quad (16)$$

$$MedAE = median(|y_i - \hat{y}_i|) \quad (17)$$

$$RMSE = \sqrt{\frac{1}{N}\sum_{i=1}^{N}(y_i - \hat{y}_i)^2} \quad (18)$$

$$R^2 = 1 - \frac{\sum_{i=1}^{N}(y_i - \hat{y}_i)^2}{\sum_{i=1}^{N}(y_i - \bar{y}_i)^2} \quad (19)$$

where y_i denotes the reference heart rate value, $\hat{y}_i$ denotes the heart rate value predicted by the model, $\bar{y}$ and $\bar{\hat{y}}$ represents the mean value of the reference and predicted heart rate data respectively, and N is the total number of test samples.

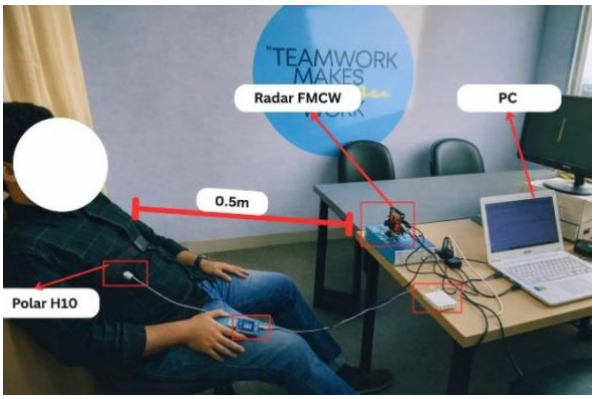

Fig. 6 Setup for self-acquired data

G. Experimental Setup

External data are utilized to evaluate the proposed model. Data sources include three subjects from a public dataset and independently acquired radar measurements. Table 2 presents the detailed radar configuration. The three subjects from the public dataset are selected due to their wide range of heart rate (HR) variability, which enhances the robustness of model evaluation. Fig. 6 illustrates the data acquisition setup for the independently collected dataset. During data acquisition, subjects are seated 0.5 meters in front of the radar and instructed to remain still for the duration of the experiment. Radar measurement results are subsequently compared with those obtained from the Polar H10, which serves as the reference sensor for HR measurement.

Table 3. Optimal Hyperparameters of the Proposed 1D-CNN Model.

Hyperparameter	Value
Pooling Type	Max pooling
Filters (Conv1–Conv6)	[96, 128, 64, 96, 96, 96]
Kernel Size (Conv1–Conv6)	[5, 7, 3, 3, 5, 5]
Dense Units	224
Learning Rate	0.001

III. Results

The proposed 1D-CNN model is evaluated on two independent datasets: a public 60 GHz dataset and a

Manuscript received 13 February 2026; Revised 6 April 2026; Accepted 8 April 2026; Available online 11 April 2026
Digital Object Identifier (**DOI**): https://doi.org/10.35882/jeeemi.v8i2.1547

self-acquired 77 GHz FMCW radar dataset. Training convergence is assessed through loss and MAE curves over 150 epochs, yielding a coefficient of determination of R^2 = 0.9629 on the test dataset. The model is benchmarked against conventional BPF- and FFT-based methods using MAE, RMSE, and MedAE. On the public 60 GHz dataset, the proposed model achieves an MAE of 6.09 BPM, RMSE of 7.34 BPM, and MedAE of 5.43 BPM, representing reductions of 66.0%, 65.5%, and 69.3% compared with the BPF baseline, respectively. On the self-acquired 77 GHz dataset, the model yields an MAE of 5.45 BPM, RMSE of 6.84 BPM, and MedAE of 4.57 BPM, corresponding to reductions of 61.2%, 62.1%, and 57.4%, respectively.

A. Model Training Result

This study employs hyperparameter optimization using Random Search with Keras Tuner, exploring filter count, kernel size, pooling type, dense layer neurons, and the Adam learning rate. The search is limited to 30 trials to minimize validation MAE. Each configuration is trained for 10 epochs, with the optimal setup detailed in Table 3.

The optimal hyperparameter configuration of the proposed 1D-CNN model is presented in Table 3. Max pooling is selected as the subsampling strategy to preserve the most salient signal features. The six convolutional layers are configured with filter sizes of [96, 128, 64, 96, 96, 96] and kernel sizes of [5, 7, 3, 3, 5, 5], forming a hierarchical architecture that progressively extracts features from broad temporal patterns to fine-grained local characteristics. A fully connected layer with 224 units is employed for regression, and the model is optimized using the Adam optimizer at a learning rate of 0.001, ensuring stable and efficient convergence.

For final training, the researchers select the optimal hyperparameter set after analyzing learning curves over 150 epochs. Both MSE and MAE losses stabilize following an initial steady decline, and experiments with 40 to 200 epochs show that extending beyond 150 epochs yields diminishing returns in validation performance. Thus, 150 epochs are sufficient to capture representative signal features without incurring unnecessary computational cost.

Training and validation loss curves are presented in Fig. 7(a), with corresponding MAE trends shown in Fig. 7(b). Both metrics decline sharply through approximately epoch 40, reflecting rapid acquisition of fundamental radar signal patterns. Beyond this point, the curves stabilize and gradually converge throughout the remainder of training. The close alignment between training and validation trajectories for both loss and MAE suggests effective generalization with minimal overfitting, even across 150 epochs. Furthermore, the model achieves a coefficient of determination of R^2 = 0.9629 on the test dataset, indicating that approximately 96.3% of the variance in reference heart rate values is captured by the proposed 1D-CNN architecture.

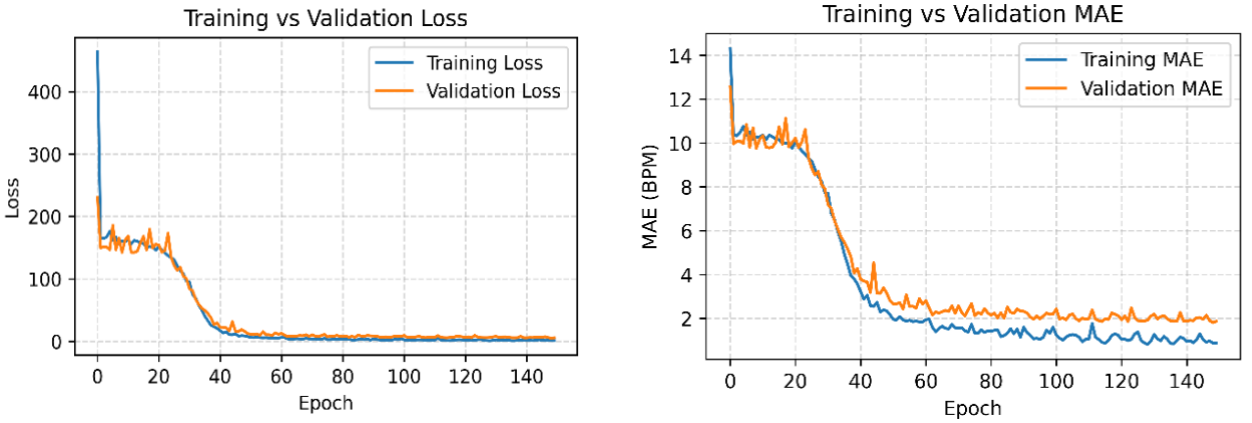

(a) (b)

Fig. 7 Comparison of training and validation (a) MAE model 1D-CNN (b) Comparison of training and validation loss model 1D-CNN

B. Heart Rate Prediction Using the 1D-CNN Model

Heart rate estimation in BPM typically relies on two conventional approaches. The first employs a bandpass filter combined with time-domain peak detection, where identified peaks are converted to HR values. The second method combines the bandpass-filtered signal with an FFT to analyze the signal in the frequency domain, referred to here as the BPF baseline approach. The dominant frequency component within the physiologically reasonable HR range is identified, and its corresponding frequency is converted to BPM by multiplying by 60 [24]. In this study, the researchers compare the proposed 1D-

Manuscript received 13 February 2026; Revised 6 April 2026; Accepted 8 April 2026; Available online 11 April 2026
Digital Object Identifier (**DOI**): https://doi.org/10.35882/jeeemi.v8i2.1547

CNN model with the conventional BPF baseline method using three complementary metrics: MAE, RMSE, and MedAE.

The performance on the public dataset is presented Table 4. Using 60–64 GHz radar data, the proposed 1D-CNN model achieved significant improvements over the BPF baseline for all error metrics. Average MAE decreases from 17.96 to 6.09 BPM, RMSE from 21.28 to 7.34 BPM, and MedAE from 17.66 to 5.43. The percentage reduction of each error metric is computed using Eq. (20).

$$Reduction = \frac{E_{baseline} - E_{proposed}}{E_{baseline}} \times 100\% \quad (20)$$

where $E_{baseline}$ denotes the error obtained from the BPF method and $E_{proposed}$ denotes the error obtained from the proposed 1D-CNN model. These absolute changes correspond to substantial BPM relative improvements: a 66.0% reduction in MAE, a 65.5% reduction in RMSE, and a 69.3% reduction in MedAE. To further evaluate the generalization capability of the proposed model, additional experiments are conducted using a dataset acquired with a radar operating in a different frequency band. Specifically, while the public dataset is collected using a 60–64 GHz radar, the independently acquired dataset employs a 77–81 GHz radar. Identical preprocessing procedures are applied to both datasets to ensure a consistent evaluation pipeline. The results from the independently acquired data are reported in Table 5. On the self-acquired dataset, the proposed model again achieves substantial error reductions: MAE decreases from 14.05 to 5.45 BPM, RMSE decreases from 18.05 to 6.84 BPM, and MedAE decreases from 10.74 to 4.57 BPM. These improvements correspond to reductions of 61.2% in MAE, 62.1% in RMSE, and 57.4% in MedAE.

A Bland–Altman analysis is employed to evaluate agreement between radar-derived heart rate estimates and reference sensor measurements. Fig. 8 presents the results for the public dataset and the self-acquired dataset. For the public dataset, as shown in Fig. 8(a), the Bland–Altman analysis yields a bias of −0.41 BPM, with 95% limits of agreement (LoA) ranging from −13.76 BPM to +12.95 BPM. This near-zero bias indicates negligible systematic deviation between the proposed method and the reference standard. The majority of data points fall within the calculated LoA boundaries and the residual scatter exhibits no apparent dependence on heart rate magnitude. These observations suggest that the 1D-CNN model achieves acceptable agreement with the reference sensor across the physiological range examined.

For the self-acquired dataset, as illustrated in Fig. 8(b), the mean error is −4.92 BPM, with LoA spanning −15.23 BPM to +5.38 BPM. This negative bias reflects a modest tendency toward underestimation relative to the reference measurements. Despite this offset, most observations remain within the LoA limits, and the distribution of differences appears consistent across the measured heart rate range. These findings indicate that, although a small constant bias exists,

Table 4. Comparison of HR estimation performance on the public dataset.

Subject	Heart Rate Range (BPM)	BPF Method			Proposed 1D-CNN Model		
		MAE	RMSE	Median AE	MAE	RMSE	Median AE
1	83-117	17.03	20.43	16.09	4.34	5.27	3.68
2	96-125	22.08	25.13	23.21	8.22	9.992	7.71
3	83-112	14.78	18.27	13.67	5.71	6.76	4.91
Average		**17.96**	**21.28**	**17.66**	**6.09**	**7.34**	**5.43**

Table 5. Comparison of HR estimation performance on the self-acquired dataset.

Subject	Heart Rate Range (BPM)	BPF Method			Proposed 1D-CNN Model		
		MAE	RMSE	Median AE	MAE	RMSE	Median AE
1	83-97	15.48	21.71	11.81	7.59	9.55	6.41
2	87-100	15.46	17.42	13	3.13	4.04	2.5
3	86-97	11.22	15.03	7.4	5.63	6.93	4.79
Average		**14.05**	**18.05**	**10.74**	**5.45**	**6.84**	**4.57**

Manuscript received 13 February 2026; Revised 6 April 2026; Accepted 8 April 2026; Available online 11 April 2026
Digital Object Identifier (**DOI**): https://doi.org/10.35882/jeeemi.v8i2.1547

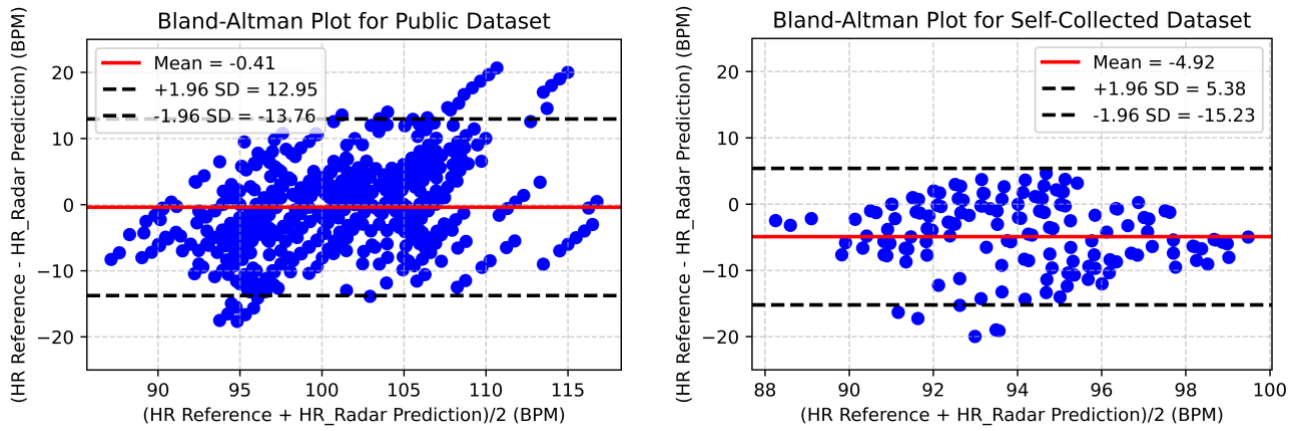

(a) (b)

Fig. 8 Bland–Altman plots comparing radar-estimated heart rate with reference measurements for (a) the public dataset and (b) the self-acquired dataset.

the model maintains stable estimation performance when applied to data acquired with different radar hardware and operating conditions.

Time-series plots from a representative test subject illustrate the estimation characteristics of each method. Fig. 9(a) presents results for the public dataset, where estimation behavior differs markedly between methods. BPF-based estimates exhibit sharper fluctuations and larger deviations from the reference signal, particularly during certain intervals. In contrast, the 1D-CNN model aligns more closely with the reference sensor, following heart rate trends more smoothly with substantially reduced amplitude discrepancy.

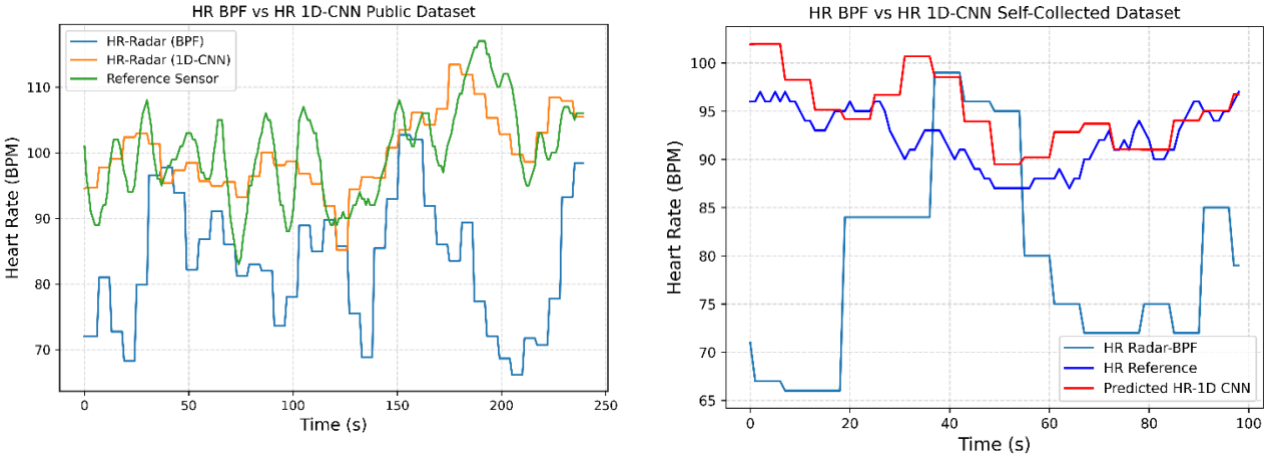

(a) (b)

Fig. 9 Comparison of heart rate estimation for one representative subject (a) the public dataset and (b) the self-acquired dataset.

Fig. 9(b) illustrates the results for the self-acquired dataset, which show a similar pattern. The BPF method, combined with FFT analysis, produces estimates with pronounced fluctuations and lower stability, likely due to weak cardiac-induced radar signals that are difficult to extract using purely frequency-domain approaches. The dominant frequency in the FFT spectrum may reflect harmonic components of chest motion or disturbances rather than the true heart rate, thereby reducing estimation accuracy. The proposed 1D-CNN model generates more stable estimates that closely track reference measurements.

C. Discussion

A. Interpretation of Model Performance and Architecture

The proposed 1D-CNN model is evaluated against conventional BPF- and FFT-based methods on two datasets. As shown in Table 4 and Table 5, the model

Manuscript received 13 February 2026; Revised 6 April 2026; Accepted 8 April 2026; Available online 11 April 2026
Digital Object Identifier (**DOI**): https://doi.org/10.35882/jeeemi.v8i2.1547

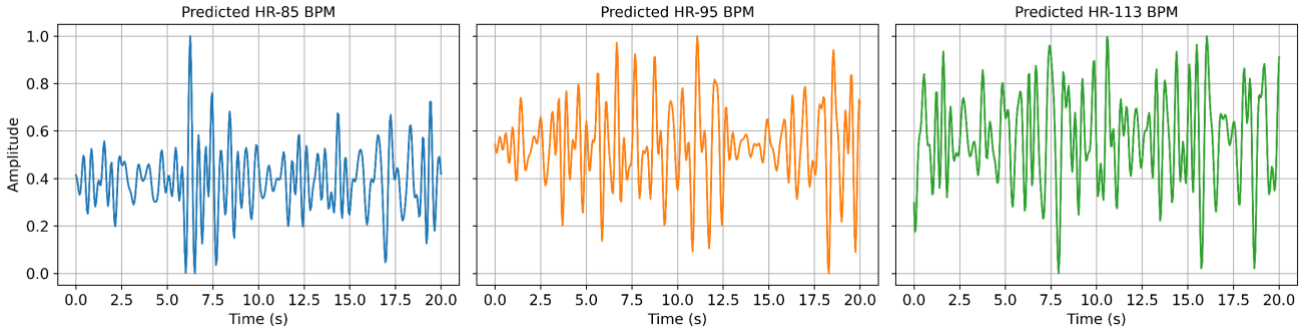

(a) (b) (c)

Fig. 10 Representative radar phase signals corresponding to different estimated heart rate values: (a) 85 BPM, (b) 95 BPM, and (c) 113 BPM

achieves an average MAE of 6.09 BPM on the public dataset and 5.45 BPM on the self-acquired dataset, compared to 17.96 BPM and 14.05 BPM produced by the BPF method, corresponding to MAE reductions of 66.1% and 61.2%, respectively. Consistent improvements are also observed in RMSE (65.5% and 62.1%) and MedAE (69.3% and 57.4%), confirming that the performance gain is robust across both datasets and all error metrics. These results indicate that the proposed model provides substantially more reliable HR estimation, particularly under conditions in which conventional spectral methods are prone to failure.

The proposed 1D-CNN model overcomes this limitation through end-to-end temporal regression. Rather than operating in the frequency domain, the model directly processes the preprocessed radar phase signal in the time domain, eliminating the need for explicit spectral peak identification. The architecture consists of six sequential Conv1D layers with kernel sizes of [5, 7, 3, 3, 5, 5] and filters of [96, 128, 64, 96, 96, 96]. Early layers (Conv1–Conv2) employ larger kernels to capture broad temporal patterns associated with heartbeat-induced chest micro-displacements. Middle layers (Conv3–Conv4) use smaller kernels with a compressed filter count to extract fine-grained local cardiac signal characteristics. Deeper layers (Conv5–Conv6) recontextualize abstract features through medium-sized kernels with stabilized filter counts to encode the global periodic structure of the heart rate signal.

The limited accuracy of the BPF method stems from its reliance on FFT-based spectral peak selection, in which the dominant frequency component within the 0.8–3 Hz band is taken as the estimated heart rate. As shown in Fig. 11, this assumption frequently fails in practice because respiratory harmonics or minor body movements can produce competing spectral peaks of comparable magnitude, causing the method to select incorrect peaks and resulting in large, abrupt estimation errors. This behavior is clinically significant, as sudden large deviations in HR estimation could lead to misinterpretation of a subject's physiological state, particularly in continuous monitoring scenarios.

As illustrated in Fig. 10, the model correctly distinguishes HR values of 85, 95, and 113 BPM by recognizing differences in inter-oscillation spacing and fluctuation density within the 20-second input window, even in the presence of amplitude variations, noise,

Table 6. Comparison with Related Studies

Reference	HR Range (BPM)	Radar	Method	HR Error Metric
Kim et al. [44]	60-120	60-64 GHz FMCW	Lightweight CNN (HeartBeatNet)	MAE = 3.82 BPM
Khan et al. [45]	-	77-81 GHZ FMCW	T-CNN	MAE = 2.37 BPM
Chang et al. [46]	-	77-81 GHZ FMCW	CNN	Absolute Error < 3 BPM
Wang et al. [47]		77-81 GHZ FMCW	CNN + Transformer	MAE = 1.82 BPM
Han-Trong et al. [48]	50-91	24 GHz CW	LSTM	Accuracy = 96.67%
This study	**88-125**	**60-64 GHz and 77-81 GHz FMCW**	**1D-CNN (Regression)**	**MAE = 6.09 and 5.45 BPM**

Manuscript received 13 February 2026; Revised 6 April 2026; Accepted 8 April 2026; Available online 11 April 2026
Digital Object Identifier (**DOI**): https://doi.org/10.35882/jeeemi.v8i2.1547

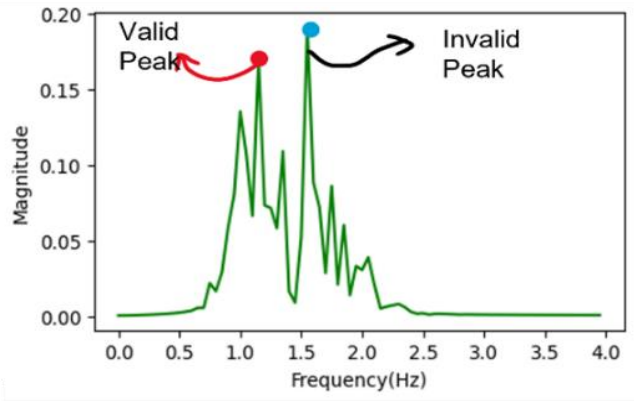

Fig. 11 The issue of invalid peak detection in the frequency domain in the BPF-based FFT method

and residual motion artifacts. This demonstrates that the model successfully captures meaningful temporal periodicity correlated with heart rate variations, suggesting its potential suitability for practical applications such as post-exercise recovery monitoring and non-contact cardiac screening, where accurate estimation within an elevated HR range is essential. The proposed 1D-CNN model addresses this limitation through a fundamentally different mechanism. Rather than operating in the frequency domain, the model receives the preprocessed radar phase signal directly as a temporal input and produces HR estimates in BPM through end-to-end regression, eliminating the need for explicit spectral peak identification.

The effectiveness of this mechanism is evident in Fig. 10, where the model correctly distinguishes between signals estimated at 85, 95, and 113 BPM by recognizing differences in inter-oscillation spacing and fluctuation density within the 20-second input window. The 85 BPM signal exhibits wider inter-oscillation intervals consistent with a longer cardiac cycle, while the 113 BPM signal displays denser fluctuations indicative of a shorter inter-beat interval. The 95 BPM signal presents intermediate temporal characteristics between the two. Notably, none of these signals conforms to an ideal sinusoidal profile due to amplitude variations, noise, and residual motion artifacts. Nevertheless, differences in oscillation density remain clearly distinguishable, confirming that the model successfully captures meaningful temporal periodicity that correlates with heart rate variations.

B. Comparison with Related Studies

Table 6 summarizes a comparison with representative related studies on FMCW radar-based HR estimation. Kim et al.[44] proposed HeartBeatNet, a lightweight CNN with skip connections and dilated convolutions operating on a 60–64 GHz FMCW radar, reporting an MAE of 3.82 BPM. Although HeartBeatNet achieves lower MAE, its multi-stage preprocessing pipeline and architectural complexity introduce greater computational overhead compared to the proposed 1D-CNN, which terminates preprocessing at the bandpass filtering stage and employs a simpler sequential architecture. Khan et al. [45] proposed a T-CNN for simultaneous heart rate and breath rate estimation using 77–81 GHz FMCW radar, achieving an MAE of 2.37 BPM with minimal preprocessing by eliminating range bin identification and respiratory harmonic filtering. However, the heart rate range of subjects was not reported, and evaluation was confined to a single radar platform. In contrast, the proposed method is validated across two frequency bands (60–64 GHz and 77–81 GHz), demonstrating broader cross-platform generalizability not addressed in prior studies.

Chang et al. [46] proposed a deep learning-aided multi-bin fusion scheme achieving an absolute error below 3 BPM, but the evaluation was limited to only three subjects and relied on a two-stage CNN with extensive preprocessing, raising concerns about generalizability. The proposed method addresses these limitations through a single-stage 1D-CNN with streamlined preprocessing, evaluated on a larger and more diverse subject pool. Wang et al. [47] proposed a CNN-Transformer hybrid with a composite loss function, achieving an MAE of 1.82 BPM on the EquiPleth dataset and 2.11 BPM on their self-acquired RadHR dataset, the lowest among the compared methods. However, evaluation was conducted solely under stationary conditions with an undisclosed heart rate range, and the hybrid architecture introduced considerable complexity unsuitable for lightweight deployment. Han-Trong et al. [48] achieved 96.67% accuracy using CW radar with LSTM, but reliance on synthetically generated training data introduced a domain gap with real physiological conditions, while dependence on dedicated hardware (ADC NI USB-6008 and LabVIEW) limited portability.

While several prior studies report lower MAE values, the proposed 1D-CNN demonstrates broader applicability through cross-platform validation across two FMCW radar frequency bands. Additionally, the model addresses an elevated heart rate range of 88–125 BPM associated with physical exertion, a condition that remains either unreported or insufficiently covered in prior studies. The adoption of a streamlined single-stage architecture further enhances its suitability for real-time and edge deployment, providing a distinct advantage over more complex multi-stage approaches. Collectively, these attributes affirm that the proposed method represents a practical and generalizable solution for radar-based heart rate monitoring across diverse operational contexts.

C. Limitations and Future Work

Manuscript received 13 February 2026; Revised 6 April 2026; Accepted 8 April 2026; Available online 11 April 2026
Digital Object Identifier (**DOI**): https://doi.org/10.35882/jeeemi.v8i2.1547

The results demonstrate that the proposed 1D-CNN model enhances heart rate estimation accuracy compared to the conventional BPF approach. However, there remains room for improvement. As shown in Table 4 and Table 5, the evaluated heart rate range is between 83 and 125 BPM. Thus, model performance at lower heart rates (60–80 BPM) is not fully evaluated. This is a notable gap, since resting-state monitoring represents one of the most common practical use cases. At lower heart rates, oscillations in the radar signal are more spread out, and it remains unclear whether the model can reliably detect these slower patterns. To address these limitations, future study focuses on incorporating additional publicly available datasets that span a broader range of heart rate values and include a larger, more diverse subject pool. Expanding the training data in this manner is expected to improve the generalization capability of the proposed model and yield more consistent estimation performance across varying physiological conditions.

V. Conclusion

This study introduces a non-contact heart rate estimation technique based on FMCW radar and 1D-CNN. The radar signal preprocessing pipeline is designed and implemented systematically. The proposed learning-based approach is evaluated against conventional bandpass filtering and FFT-based peak detection methods. Experimental results show that the 1D-CNN model provides more accurate and stable heart rate estimations than traditional frequency-domain approaches. The model reduces MAE, RMSE, and MedAE from 17.96, 21.28, and 17.66 BPM to 6.09, 7.34, and 5.43 BPM, respectively, on the public dataset, while achieving consistent gains on the independent dataset with errors decreasing from 14.05, 18.05, and 10.74 BPM to 5.45, 6.84, and 4.57 BPM. These results indicate improved robustness against noise, spectral overlaps, and signal interference. The method is validated using two radar systems operating at 60–64 GHz and 77–81 GHz, both employing identical preprocessing procedures. Consistent performance improvements across different radar frequencies and datasets confirm the reliability and generalization capability of the proposed method. Moreover, a comparative analysis with related studies further demonstrates that the regression-based 1D-CNN achieves lower MAE values than previously reported filtering- and FFT-based methods, even when evaluated across a higher heart rate range (83–125 BPM). This result highlights the model's ability to learn nonlinear temporal patterns in radar phase signals without relying solely on a dominant spectral peak. In summary, a data-driven regression framework based on 1D-CNN is more suitable for FMCW radar-based heart rate estimation than conventional peak-selection techniques. This validation focuses on heart rates between 83 and 125 BPM under quasi-static conditions. Future work expands the dataset to include lower heart rate ranges, motion artifacts, and dynamic real-world scenarios. These steps help evaluate the robustness and clinical applicability of the proposed system.

Acknowledgments

The researchers would like to express their gratitude to the Department of Electrical Engineering, Telkom University, particularly the Signal Processing and Learning for Spatial Intelligence (SPELL) Laboratory, as well as to the other contributors for their support and contributions to the development of the algorithms and the completion of this study.

Funding

This study receives no specific grant from any funding agency in the public, commercial, or not-for-profit sectors.

Data Availability

a) The public FMCW radar dataset was collected from (https://doi.org/10.6084/m9.figshare.13515977.v1)[34].
b) The self-acquired FMCW radar dataset is generated in this study and is available at GitHub: (https://github.com/Diyah-Widiya/Dataset-FMCW-Radar-IWR1843).

Author Contribution

Diyah Widiyasari was responsible for study conceptualization, experimental design, data acquisition, and signal processing. Istiqomah contributed to the development of the machine learning algorithms. Fiky Yosef Suratman contributed to the editing and revision of the manuscript. Suto Setiyadi assisted in data acquisition and data management. All authors read and approved the final manuscript and took full responsibility for the integrity of the study.

Declarations

Ethical Approval

The researchers confirm that all ethical guidelines for publication in *Data in Brief* are strictly followed. The study involves human participants, and written informed consent is obtained from all participants prior to data acquisition for the collection, use, and publication of the data. The self-acquired dataset does not include any personal, identifiable, or sensitive information that could compromise participant privacy. Therefore, formal ethical approval is not required for this study.

Manuscript received 13 February 2026; Revised 6 April 2026; Accepted 8 April 2026; Available online 11 April 2026
Digital Object Identifier (**DOI**): https://doi.org/10.35882/jeeemi.v8i2.1547

Consent for Publication Participants
Consent for publication is provided by all participants.

Competing Interests
The researchers declare no competing interests.

References

[1] A. Hassanpour and B. Yang, "Contactless Vital Sign Monitoring: A Review Towards Multi-Modal Multi-Task Approaches," *Sensors*, vol. 25, no. 15, 2025, doi: 10.3390/s25154792.

[2] X. Huang, Z. Ju, and R. Zhang, "Real-Time Heart Rate Detection Method Based on 77 GHz FMCW Radar," *Micromachines (Basel).*, vol. 13, no. 11, 2022, doi: 10.3390/mi13111960.

[3] S. Mun, K. Park, J.-K. Kim, J. Kim, and S. Lee, "Assessment of heart rate measurements by commercial wearable fitness trackers for early identification of metabolic syndrome risk.," *Sci. Rep.*, vol. 14, no. 1, p. 23865, Oct. 2024, doi: 10.1038/s41598-024-74619-7.

[4] A. Freitas, R. Almeida, H. Gonçalves, G. Conceição, and A. Freitas, "Monitoring fatigue and drowsiness in motor vehicle occupants using electrocardiogram and heart rate − A systematic review," *Transp. Res. Part F Traffic Psychol. Behav.*, vol. 103, pp. 586–607, 2024, doi: https://doi.org/10.1016/j.trf.2024.05.008.

[5] A. Galli, R. J. H. Montree, S. Que, E. Peri, and R. Vullings, "An Overview of the Sensors for Heart Rate Monitoring Used in Extramural Applications.," *Sensors (Basel)*, vol. 22, no. 11, May 2022, doi: 10.3390/s22114035.

[6] Y. Chen, J. Yuan, and J. Tang, "A high precision vital signs detection method based on millimeter wave radar," *Sci. Rep.*, vol. 14, no. 1, p. 25535, 2024, doi: 10.1038/s41598-024-77683-1.

[7] A. El Abbaoui, D. Sodoyer, and F. Elbahhar, "Contactless Heart and Respiration Rates Estimation and Classification of Driver Physiological States Using CW Radar and Temporal Neural Networks," *Sensors*, vol. 23, no. 23, 2023, doi: 10.3390/s23239457.

[8] N. Roy and Z. Hasan, "Contactless Physiological Health Sensing: Challenges, Solutions & Opportunities," in *2024 IEEE International Conference on Smart Computing (SMARTCOMP)*, 2024, p. 3. doi: 10.1109/SMARTCOMP61445.2024.00020.

[9] D. Kolosov, V. Kelefouras, P. Kourtessis, and I. Mporas, "Contactless Camera-Based Heart Rate and Respiratory Rate Monitoring Using AI on Hardware," *Sensors*, vol. 23, no. 9, 2023, doi: 10.3390/s23094550.

[10] W. Xue, R. Wang, L. Liu, and D. Wu, "Accurate multi-target vital signs detection method for FMCW radar," *Measurement*, vol. 223, p. 113715, 2023.

[11] M. Xiang, W. Ren, W. Li, Z. Xue, and X. Jiang, "High-Precision Vital Signs Monitoring Method Using a FMCW Millimeter-Wave Sensor," *Sensors*, vol. 22, no. 19, p. 7543, 2022.

[12] F. Yang, S. He, S. Sadanand, A. Yusuf, and M. Bolic, "Contactless Measurement of Vital Signs Using Thermal and RGB Cameras: A Study of COVID 19-Related Health Monitoring," *Sensors*, vol. 22, no. 2, 2022, doi: 10.3390/s22020627.

[13] S. Yao *et al.*, "Radar-Camera Fusion for Object Detection and Semantic Segmentation in Autonomous Driving: A Comprehensive Review," *IEEE Transactions on Intelligent Vehicles*, vol. 9, no. 1, pp. 2094–2128, 2024, doi: 10.1109/TIV.2023.3307157.

[14] A. Singh, S. U. Rehman, S. Yongchareon, and P. H. J. Chong, "Multi-Resident Non-Contact Vital Sign Monitoring Using Radar: A Review," *IEEE Sens. J.*, vol. 21, pp. 4061–4084, 2021, [Online]. Available: https://api.semanticscholar.org/CorpusID:229191649

[15] T. Wu, T. S. Rappaport, and C. M. Collins, "Safe for Generations to Come.," *IEEE Microw. Mag.*, vol. 16, no. 2, pp. 65–84, Mar. 2015, doi: 10.1109/MMM.2014.2377587.

[16] S. Marty, F. Pantanella, A. Ronco, K. Dheman, and M. Magno, "Investigation of mmWave Radar Technology For Non-contact Vital Sign Monitoring," in *2023 IEEE International Symposium on Medical Measurements and Applications (MeMeA)*, 2023, pp. 1–6. doi: 10.1109/MeMeA57477.2023.10171940.

[17] G. Paterniani *et al.*, "Radar-Based Monitoring of Vital Signs: A Tutorial Overview," *Proceedings of the IEEE*, vol. 111, no. 3, pp. 277–317, 2023, doi: 10.1109/JPROC.2023.3244362.

[18] H.-S. Cho and Y.-J. Park, "UWB Radar-Based Human Activity Recognition via EWT–Hilbert Spectral Videos and Dual-Path Deep Learning," *Electronics (Basel).*, vol. 14, no. 16, 2025, doi: 10.3390/electronics14163264.

[19] Z. Shen, J. Nunez-Yanez, and N. Dahnoun, "Advanced Millimeter-Wave Radar System for Real-Time Multiple-Human Tracking and Fall Detection," *Sensors*, vol. 24, no. 11, 2024, doi: 10.3390/s24113660.

[20] A. Kanakapura Sriranga, Q. Lu, and S. Birrell, "Enhancing Heart Rate Detection in Vehicular

Manuscript received 13 February 2026; Revised 6 April 2026; Accepted 8 April 2026; Available online 11 April 2026
Digital Object Identifier (**DOI**): https://doi.org/10.35882/jeeemi.v8i2.1547

Settings Using FMCW Radar and SCR-Guided Signal Processing," *Sensors*, vol. 25, no. 18, 2025, doi: 10.3390/s25185885.

[21] G. Lei, W. Cheng, X. Yin, and Y. Wu, "An innovative approach for FMCW radar vital sign monitoring with removal of respiratory harmonics," *Digit. Signal Process.*, vol. 157, p. 104911, 2025, doi: https://doi.org/10.1016/j.dsp.2024.104911.

[22] Y. Wang, W. Wang, M. Zhou, A. Ren, and Z. Tian, "Remote monitoring of human vital signs based on 77-GHz mm-wave FMCW radar," *Sensors*, vol. 20, no. 10, p. 2999, 2020.

[23] H. Xu, M. P. Ebrahim, K. Hasan, F. Heydari, P. Howley, and M. R. Yuce, "Accurate Heart Rate and Respiration Rate Detection Based on a Higher-Order Harmonics Peak Selection Method Using Radar Non-Contact Sensors," *Sensors*, vol. 22, no. 1, 2022, doi: 10.3390/s22010083.

[24] Z. Hao, Y. Wang, F. Li, G. Ding, K. Fan, and Y. Gao, "Detection of vital signs based on millimeter wave radar," *Sci. Rep.*, vol. 15, no. 1, p. 28112, 2025, doi: 10.1038/s41598-025-09112-w.

[25] J. Cui, Y. Liu, and H. Zheng, "Respiration and Heart Rate Detection for Human Dynamic Monitoring Based on Millimeter-wave Radar," in *Proceedings of the 2024 International Conference on Image Processing, Multimedia Technology and Maching Learning*, in IPMML '24. New York, NY, USA: Association for Computing Machinery, 2025, pp. 230–235. doi: 10.1145/3722405.3722442.

[26] W. Lv, W. He, X. Lin, and J. Miao, "Non-Contact Monitoring of Human Vital Signs Using FMCW Millimeter Wave Radar in the 120 GHz Band," *Sensors*, vol. 21, no. 8, 2021, doi: 10.3390/s21082732.

[27] L. Yuan and M. Liu, "FMCW Radar Vital Signs Detection Based on GMFD Algorithm," in *Proceedings of the 2nd International Conference on Artificial Intelligence of Things and Computing*, in AITC '25. New York, NY, USA: Association for Computing Machinery, 2025, pp. 84–89. doi: 10.1145/3762329.3762345.

[28] J. Saluja, J. Casanova, and J. Lin, "A Supervised Machine Learning Algorithm for Heart-Rate Detection Using Doppler Motion-Sensing Radar," *IEEE J. Electromagn. RF Microw. Med. Biol.*, vol. 4, no. 1, pp. 45–51, 2019.

[29] W. Zhao and G. Tong, "A deep learning based heart rate estimation method for millimeter wave radar," *Measurement*, vol. 255, p. 117923, 2025, doi: https://doi.org/10.1016/j.measurement.2025.117923.

[30] A. O. Ige and M. Sibiya, "State-of-the-Art in 1D Convolutional Neural Networks: A Survey," *IEEE Access*, vol. 12, pp. 144082–144105, 2024, doi: 10.1109/ACCESS.2024.3433513.

[31] F. Khan, X. Yu, Z. Yuan, and A. U. Rehman, "ECG classification using 1-D convolutional deep residual neural network.," *PLoS One*, vol. 18, no. 4, p. e0284791, 2023, doi: 10.1371/journal.pone.0284791.

[32] H. Narotamo, M. Dias, R. Santos, A. V Carreiro, H. Gamboa, and M. Silveira, "Deep learning for ECG classification: A comparative study of 1D and 2D representations and multimodal fusion approaches," *Biomed. Signal Process. Control*, vol. 93, p. 106141, 2024, doi: https://doi.org/10.1016/j.bspc.2024.106141.

[33] K. E. Ch Vidyasagar, K. Revanth Kumar, G. N. K. Anantha Sai, M. Ruchita, and M. J. Saikia, "Signal to Image Conversion and Convolutional Neural Networks for Physiological Signal Processing: A Review," *IEEE Access*, vol. 12, pp. 66726–66764, 2024, doi: 10.1109/ACCESS.2024.3399114.

[34] S. Yoo *et al.*, "Radar recorded child vital sign public dataset and deep learning-based age group classification framework for vehicular application," *Sensors*, vol. 21, no. 7, p. 2412, 2021.

[35] A. S. D. Lopes, "Bio-radar applications for remote vital signs monitoring," Universidade NOVA de Lisboa (Portugal), 2020.

[36] L. A. López-Valcárcel, M. García Sánchez, F. Fioranelli, and O. A. Krasnov, "An MTI-Like Approach for Interference Mitigation in FMCW Radar Systems," *IEEE Trans. Aerosp. Electron. Syst.*, vol. 60, no. 2, pp. 1985–2000, 2024, doi: 10.1109/TAES.2023.3345263.

[37] J. Wei, L. Huang, P. Tong, B. Tan, J. Bai, and Z. Wu, "Realtime Multi-target Vital Sign Detection with 79GHz FMCW Radar," in *2020 IEEE MTT-S International Wireless Symposium (IWS)*, 2020, pp. 1–3. doi: 10.1109/IWS49314.2020.9359969.

[38] D. Wang, S. Yoo, and S. H. Cho, "Experimental comparison of IR-UWB radar and FMCW radar for vital signs," *Sensors*, vol. 20, no. 22, p. 6695, 2020.

[39] D. Xu, W. Yu, C. Deng, and Z. S. He, "Non-Contact Detection of Vital Signs Based on Improved Adaptive EEMD Algorithm (July 2022)," *Sensors*, vol. 22, no. 17, 2022, doi: 10.3390/s22176423.

[40] K. S. Quigley, P. J. Gianaros, G. J. Norman, J. R. Jennings, G. G. Berntson, and E. J. C. de Geus, "Publication guidelines for human heart

Manuscript received 13 February 2026; Revised 6 April 2026; Accepted 8 April 2026; Available online 11 April 2026
Digital Object Identifier (**DOI**): https://doi.org/10.35882/jeeemi.v8i2.1547

rate and heart rate variability studies in psychophysiology—Part 1: Physiological underpinnings and foundations of measurement," *Psychophysiology*, vol. 61, no. 9, p. e14604, 2024.

[41] A. Lopes, D. F. N. Osório, H. Silva, and H. Gamboa, "Equivalent Pipeline Processing for IR-UWB and FMCW Radar Comparison in Vital Signs Monitoring Applications," *IEEE Sens. J.*, vol. 22, no. 12, pp. 12028–12035, 2022, doi: 10.1109/JSEN.2022.3173218.

[42] J. Brandstetter, E.-M. Knoch, and F. Gauterin, "Heart Rate Estimation Using FMCW Radar: A Two-Stage Method Evaluated for In-Vehicle Applications," *Biomimetics*, vol. 10, no. 9, 2025, doi: 10.3390/biomimetics10090630.

[43] S. Kiranyaz, O. Avci, O. Abdeljaber, T. Ince, M. Gabbouj, and D. J. Inman, "1D convolutional neural networks and applications: A survey," *Mech. Syst. Signal Process.*, vol. 151, p. 107398, 2021, doi: https://doi.org/10.1016/j.ymssp.2020.107398.

[44] D. Kim, J. Choi, J. Yoon, S. Cheon, and B. Kim, "HeartBeatNet: Enhancing Fast and Accurate Heart Rate Estimation With FMCW Radar and Lightweight Deep Learning," *IEEE Sens. Lett.*, vol. 8, no. 4, pp. 1–4, 2024, doi: 10.1109/LSENS.2024.3378199.

[45] A. Khan, M. Wajid, A. Srivastava, H. K. Meena, and O. Farooq, "Contactless Vital Sign Monitoring on Edge Devices with Low-Complexity T-CNN and mmWave FMCW Radar," *IEEE Sens. J.*, 2025.

[46] H. Y. Chang, C. H. Hsu, and W. H. Chung, "Fast Acquisition and Accurate Vital Sign Estimation with Deep Learning-Aided Weighted Scheme Using FMCW Radar," *IEEE Vehicular Technology Conference*, vol. 2022-June, 2022, doi: 10.1109/VTC2022-Spring54318.2022.9860799.

[47] Y. Wang, Z. Sun, X. Cheng, and Z. He, "CNN-Transformer Framework with Hybrid Loss for Robust FMCW Radar-based Heartbeat Sensing," 2025.

[48] T. Han-Trong and H. Nguyen Viet, "An Efficient Heart Rate Measurement System Using Medical Radar and LSTM Neural Network," *Journal of Electrical and Computer Engineering*, vol. 2022, 2022, doi: 10.1155/2022/4696163.

Author Biography

Diyah Widiyasari received the bachelor's degree in electrical engineering from Institut Teknologi Sumatera in 2021 and the master's degree in electrical engineering from Institut Teknologi Bandung in 2023. During her academic journey, she has been actively engaged in various research activities, particularly radar signal processing, embedded systems, and hardware design. Her current research interests include the development of signal processing algorithms for radar applications, hardware–software co-design in field-programmable gate arrays (FPGA) and SoC platforms, and the creation of smart devices that integrate various sensors with machine learning techniques. In addition to her research activities, she currently serves as a lecturer in the Department of Electrical Engineering at Telkom University.

Istiqomah received the bachelor's degree from Telkom University, Bandung, and the master's degree from the National Chiao Tung University (NCTU), Taiwan, specializing in electrical and computer engineering. She is a dedicated and accomplished professional in electrical and computer engineering. Since 2020, she has been a lecturer in the Department of Electrical Engineering at Telkom University. Her research interests include cutting-edge fields such as Artificial Intelligence of Things (AIoT), human activity recognition, machine learning, and deep learning. With a strong academic foundation and a passion for innovation, she is at the forefront of technological advancements in her field.

Fiky Y.Suratman (Member, IEEE) was born in Jakarta, Indonesia, in 1976. He received the bachelor's degree in engineering physics and the master's degree from the School of Electrical and Informatics (STEI), Institut Teknologi Bandung, Bandung, Indonesia, in 1998 and 2006, respectively, and the Dr.-Ing. degree from Technische Universitaet Darmstadt (TU Darmstadt), Darmstadt, Germany, in 2014. He had an early placement in industry at Astra Microtronics Technology, Batam, Indonesia, from 1998 to 2001. In 2007, he joined the Faculty of Electrical Engineering, Telkom University, Bandung, as a faculty member. He served as the Head of the Department of Electrical Engineering, Telkom University from 2014 to 2023. His research interests include statistical signal processing, radar signal processing, and machine learning. Dr.

Manuscript received 13 February 2026; Revised 6 April 2026; Accepted 8 April 2026; Available online 11 April 2026
Digital Object Identifier (**DOI**): https://doi.org/10.35882/jeeemi.v8i2.1547

Suratman is a member of the IEEE Signal Processing Society.

Suto Setiyadi received the bachelor's degree from Telkom University, Indonesia, in 2021, and the master's degree from the same university in 2023. He currently serves as a lecturer and researcher at the School of Electrical Engineering, Telkom University. He is the author of the textbook *Sensor and Actuator with the Cases of Implementation* (Tel-U Press, 2022). His research interests include biomedical applications of computer vision and embedded systems.

Manuscript received 13 February 2026; Revised 6 April 2026; Accepted 8 April 2026; Available online 11 April 2026
Digital Object Identifier (**DOI**): https://doi.org/10.35882/jeeemi.v8i2.1547